Study on Large-Scale Amplitude Modulation of Near-Wall Small-Scale Structures in Turbulent Wall-Bounded Flows

Esther Mäteling$^{(\boxtimes)}$, Michael Klaas, and Wolfgang Schröder

Chair of Fluid Mechanics and Institute of Aerodynamics, Wüllnerstraße 5a, 52062 Aachen, Germany
e.maeteling@aia.rwth-aachen.de

Abstract. Recently, a novel approach to study the inner-outer interactions in turbulent wall-bounded flows has been presented by Mäteling et al. [8], which tackles the combined effects of superposition, bursting events, and amplitude modulation based on the time-dependent streamwise velocity fluctuations. This approach is extended in the current study to all three velocity fluctuation components. Due to the incorporation of the wall-normal velocity fluctuations, the bursting events can be study in more detail and independently of the superposition. By using a multivariate empirical mode decomposition for the scale separation, all velocity components at both wall-normal positions can be decomposed simultaneously to ensure proper scale alignment between the resulting modal representations. The results show that the superposition effect and the amplitude modulation exist in all three velocity components but are most intense for the streamwise fluctuations. A high level of coherence of the sweeps and ejections is also detected by conventional cross-correlation.

Keywords: Amplitude modulation · Scale interaction mechanisms · Turbulent wall-bounded flow

1 Introduction

The interaction between outer-layer large-scale structures and near-wall turbulence has been a subject of turbulence research for the past decades. Aiming at a deeper understanding of the internal structure of turbulent wall-bounded flows, the inner-outer coherence seems to play a fundamental part in the energy and momentum exchange of flow structures of different scales. Yet, four phenomena have been assigned to this structural interaction, which are superposition, bursting events, amplitude modulation, and frequency modulation. The interested reader is referred to the excellent reviews of [4,7] concerning this topic.

In a recent study, Mäteling et al. [8] introduced a novel approach to investigate the combined effects of superposition, bursting events, and amplitude modulation. They used time-dependent one-dimensional (1D) streamwise velocity

fluctuations at an inner- and an outer-layer position of a direct numerical simulation (DNS) of a turbulent channel flow (TCF) at a friction Reynolds number $Re_\tau \approx 1000$. By removing the influences of superposition and bursting events prior to performing the analysis of amplitude modulation, the latter could be revealed in a very clear manner. This is additionally achieved by a modified algorithm to calculate the large-scale amplitudes. They are directly obtained from the large scales after performing a second scale separation instead of the conventionally used large-scale trend of the small-scale amplitudes [1,9].

The current study extends the approach of Mäteling et al. [8] to all three velocity fluctuation components. This additionally enables a separate, in-depth investigation of superposition and bursts since the bursting events can now be defined based on the signs of streamwise and wall-normal fluctuations using quadrant analysis. The authors of [8] showed that a scale separation by empirical mode decomposition (EMD) and by spectral filtering yields similar outcomes of the interaction analysis. In the present analysis, an extension of the univariate EMD to multiple variates by Rehman & Mandic [11] is applied. This multivariate EMD (MEMD) enables a simultaneous decomposition of all velocity components at both wall-normal positions, which ensures a proper scale alignment between individual modes. The spectral alignment guarantees that the same scales are assigned to the large scales at the near-wall and the outer-layer position, which increases the precision of the subsequent inner-outer interaction analysis.

In the following, the DNS data of the TCF are presented in Sect. 2. Then, the methods for scale separation and for revealing the interaction mechanisms between the outer-layer and the near-wall signals are outlined in Sect. 3. The results are shown in Sect. 4 and conclusions are drawn in Sect. 5.

2   Data Set

The present study uses DNS data of a TCF at $Re_\tau = \frac{u_\tau h}{\nu} \approx 1000$, where u_τ is the friction velocity, h the channel half height, and ν the kinematic viscosity. The simulation data are provided by the *Johns Hopkins Turbulence Database* [2] and comprise a domain of $(L_x \times L_y \times L_z) = (8\pi h \times 2h \times 3\pi h)$ with $h = 1$ and $(2048 \times 512 \times 1536)$ nodes. The cell sizes measure $(\Delta x^+ \times \Delta y^+ \times \Delta z^+) = (12.2639 \times 1.65199 \cdot 10^{-2}$ (at the wall) -6.15507 (at the centerline) $\times 6.13196)$.

For the current investigation, 1D time-dependent signals at a fixed streamwise and spanwise position are extracted at two wall-normal locations. The near-wall velocity fluctuations are taken at $y_{NW}^+ = 1$ and the outer-layer fluctuations are extracted at $y_{OL}^+ = 123$, where the large-scale motions are most energetic according to $y_{OL}^+ = 3.9\sqrt{Re_\tau}$ [6]. In total, 4000 time steps with a spacing of $\Delta t^+ = 0.325$ are available, which results in a total temporal length of $t^+ \approx 1300$. The temporal resolution is comparable to hot-wire anemometry data that is often used to study inner-outer interactions, e.g., [10]. For more information about the DNS data set, the reader is referred to [2].

Throughout this paper, the superscript + indicates quantities scaled by inner units, i.e., by u_τ and ν. The index LS indicates large scales. A near-wall signal

is denoted by the index NW, an outer-layer location is defined by OL, and the symbol ˆ marks an amplitude.

3   Methodical Approach

3.1   Multivariate Empirical Mode Decomposition

When applying EMD for scale separation in the inner-outer interaction analysis, past studies, e.g., [1,8], used its univariate form originally introduced by Huang et al. [3]. This data-driven algorithm decomposes a non-linear, time-dependent signal into Intrinsic Mode Functions (IMFs), which are solely based on the signal's characteristics. Further information of its features and application to fluid flow data can be found in, e.g., [8]. However, this method has some disadvantages, which certainly influence the precision of the interaction analysis. Since velocity signals at different wall-normal locations usually possess individual characteristics, a varying number of decomposition levels, i.e., a different number of IMFs, is obtained when applying the univariate EMD. In addition, mode mixing occurs, which is a consequence of signal intermittency causing an overlapping of the mode spectra. These effects lead to improper mode alignment and complicate a comparison of individual IMFs at the considered near-wall and outer-layer location as it is done to study the inner-outer interactions.

To overcome these drawbacks, which also play a major role in various physics-related applications of EMD, Rehman & Mandic developed a multivariate extension (MEMD), which simultaneously decomposes multi-channel temporal signals [11]. The authors utilized real-valued signal projections to tackle the challenging definition of local extrema in multivariate data, which is a key step to determine the local mean during the sifting process. The main steps of the algorithm are outlined in the following based on the description found in [11].

1. Selection of a suitable low-discrepancy point set, e.g., a Hammersley sequence, for sampling on an $(n-1)$ sphere, where n denotes the number of variates. The point set defines the angles φ_k, with k being the projection directions, from which the unit projection vectors $p^{\varphi_k}(t)$ are obtained.
2. Projection of the multivariate input signal $I(t)$ on $p^{\varphi_k}(t)$, which is denoted by $P^{\varphi_k}(t)$.
3. Determination of the locations of the local extrema of each projection $P^{\varphi_k}(t)$.
4. Interpolation of the original signal $I(t)$ at these extrema locations yields the mean envelopes $e^{\varphi_k}(t)$.
5. Averaging the envelopes $e^{\varphi_k}(t)$ over all projection directions gives the local mean envelope $m(t)$.
6. Extraction of the detail $d(t)$ using $I(t)$ - $m(t)$. If the detail fulfills the stoppage criterion for a multivariate IMF [11], the first IMF equals $d(t)$ and the above procedure is applied to $I(t)$ - $d(t)$. Otherwise, the sifting is proceeded with $d(t)$.

The interested reader is referred to [11] for more details about the MEMD algorithm. For the current analysis, six variates $(u', v', w'$ at y^+_{NW} and at $y^+_{OL})$ are simultaneously decomposed using 22 projection directions. The first six IMFs are assigned to the small scales and the remaining modes to the large scales.

3.2   Inner-Outer Interaction Analysis

The three phenomena of superposition, bursting activity, and amplitude modulation are investigated with respect to the inner-outer interaction. The procedure described in [8] is adapted to all three velocity components and due to the lack of space, only a rough outline and the variations to the original approach are given in the following. The reader is referred to [8] for in-depth physical and mathematical foundations of the analysis.

Besides the application of the MEMD, a main difference of the current study is the separate investigation of superposition and bursts. Therefore, the large-scale components of all three velocity fluctuations at y^+_{NW} and y^+_{OL} - obtained by MEMD - are correlated by standard cross-correlation (Eq. 1 with $q' = \{u', v', w'\}$) to analyze the superposition. Additionally, based on quadrant analysis, the large-scale streamwise and wall-normal components that either indicate sweeps or ejections are separately correlated (Eq. 1 with $q' = \{q'_{sw}, q'_{ej}\}$). Therefore, the streamwise and the wall-normal fluctuations of both events are combined to complex numbers prior to performing the cross-correlation.

$$R_i\left(\Delta t^+\right) = \frac{\overline{q'_{NW,LS}\left(t^+\right) \cdot \overline{q'_{OL,LS}\left(t^+ + \Delta t^+\right)}}}{\sqrt{q'^2_{NW,LS}\left(t^+\right)} \cdot \sqrt{q'^2_{OL,LS}\left(t^+ + \Delta t^+\right)}} \tag{1}$$

The outer-layer large-scale influence is subsequently removed from all three near-wall velocity components. The event-specific strength of correlation $R_{i,max}$ as well as the inclination angle

$$\Theta_i = tan^{-1}\left(\frac{\Delta y^+_{NW-OL}}{\Delta x^+_i}\right) \tag{2}$$

are thereby considered. The difference Δy^+_{NW-OL} corresponds to the wall-normal distance between inner and outer layer, while Δx^+_i is the spatial shift obtained from Δt^+_i via Taylor's hypothesis. The remaining near-wall signals with $q' = \{u', v', w'\}$ are calculated by

$$\begin{aligned}
q'_{NW,woSB}(t^+) = q'_{NW}(t^+) &- R_{S,q',max} \cdot q'_{OL,LS}(t^+, \Theta_{S,q'})\\
&- R_{sw,max} \cdot q'_{OL,LS,sw}(t^+, \Theta_{sw})\\
&- R_{ej,max} \cdot q'_{OL,LS,ej}(t^+, \Theta_{ej}).
\end{aligned} \tag{3}$$

With respect to the bursts, only the streamwise (wall-normal) component is subtracted from the streamwise (wall-normal) near-wall signal and the spanwise near-wall fluctuations are certainly not affected by bursting activity.

A second MEMD is applied to the remaining near-wall signals and the unchanged outer-layer fluctuations. Using the Hilbert transform with $q' = \{u', v', w'\}_{NW,OL}$

$$q'_{HT,LS2}\left(t^+\right) = \frac{P}{\pi} \int_{-\infty}^{\infty} \frac{q'_{LS2}\left(t^\star\right)}{t - t^\star} dt^\star, \tag{4}$$

imaginary components are determined to build an analytic signal from each large-scale component, which enables the calculation of the large-scale amplitudes via

$$\hat{q}'_{LS2}\left(t^+\right) = \sqrt{q'^2_{LS2}\left(t^+\right) + q'^2_{HT,LS2}\left(t^+\right)}. \tag{5}$$

They are correlated for the amplitude modulation analysis by standard cross-correlation (Eq. 1 with $q' = \{\hat{u}', \hat{v}', \hat{w}'\}$).

4   Results

The large-scale components obtained by MEMD are shown in Fig. 1 for all three velocity components and the bursting events. They are scaled by the corresponding rms values to obtain comparable fluctuation values. All distributions possess a similar trend between the near-wall and the outer-layer scales. Local extrema of the outer large scales are often found in the near-wall signals but with a temporal shift and a varying strength. Particularly for the wall-normal fluctuations (Fig. 1b), an offset occurs between near-wall and outer-layer distribution. The near-wall bursting events shown in Fig. 1d often possess a shorter lifetime compared to their outer-layer counterparts.

To quantify the degree of inner-outer interaction, the large-scale components shown in Fig. 1 are cross-correlated. The resulting correlation functions R_i are given in Fig. 2 as a function of the time shift Δt^+. The permitted shifts along the positive and the negative time axis comprise inclination angles in the range $\Theta_i \geq \pm 1.27°$. From Fig. 2a it is obvious that the superposition of the streamwise fluctuations is most intense with a maximum correlation coefficient of $R_{S,u,max} = 0.69$. The value is similar to the coefficients reported in the literature [5,10]. The wall-normal correlation is quite low with $R_{S,v,max} = 0.16$ and the spanwise correlation features two distinct peaks of which the slightly higher peak indicates $R_{S,w,max} = 0.28$. This somehow shows the limitations of classical cross-correlation when applied to fluctuation values. Although an inner-outer coherence is visible in Fig. 1 with the naked eye for all velocity components, the correlation does not reflect this effect. Particularly for the wall-normal fluctuations, this is caused by the offset between inner and outer distribution, which often leads to opposed signs that falsify the correlation results. Hence, alternative approaches should be developed in the future for a more accurate determination of the inner-outer correlation.

Figure 2b shows high maximum correlation values for the bursting events. The sweeps' peak correlation measures $R_{sw,max} = 0.68$ and the value of the ejections is slightly lower with $R_{ej,max} = 0.63$. These values are thus comparable
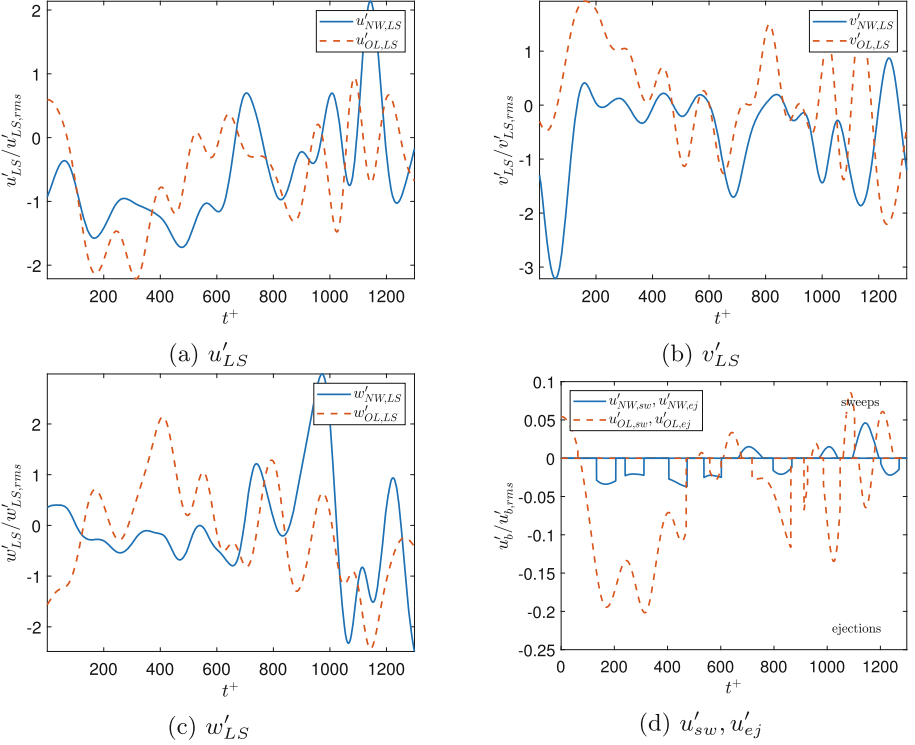
(a) u'_{LS}

(b) v'_{LS}

(c) w'_{LS}

(d) u'_{sw}, u'_{ej}

Fig. 1. Near-wall $\{u, u_b, v, w\}'_{NW,LS}$ and outer-layer large-scale signals $\{u, u_b, v, w\}'_{OL,LS}$.

to the superposition of the streamwise fluctuations. Since the signs of near-wall and outer-layer features are always the same, the above addressed drawback of the cross-correlation method does not appear for the bursts.

All maximum correlation values and the corresponding inclination angles are summarized in Table 1. While the superposition of streamwise and wall-normal fluctuations indicates a similar inclination angle around $\Theta_S \approx 8°$, the spanwise correlation has a lower angle of $\Theta_{S,w} = 2.4°$. A more surprising deviation occurs for the bursting events. The sweeping interaction possesses a negative angle, which indicates leading near-wall activity, and the ejections are characterized by a very high angle, i.e., only a small shift between inner and outer ejections. This demands for further analysis with an extended data range that is beyond the scope of the current study.

In a subsequent step, the outer-layer influences are removed from the near-wall signals. Afterwards, the remaining near-wall and the unchanged outer-layer signals are decomposed by MEMD yielding "updated" large scales. The amplitudes of these large scales are determined from the analytic signals and are
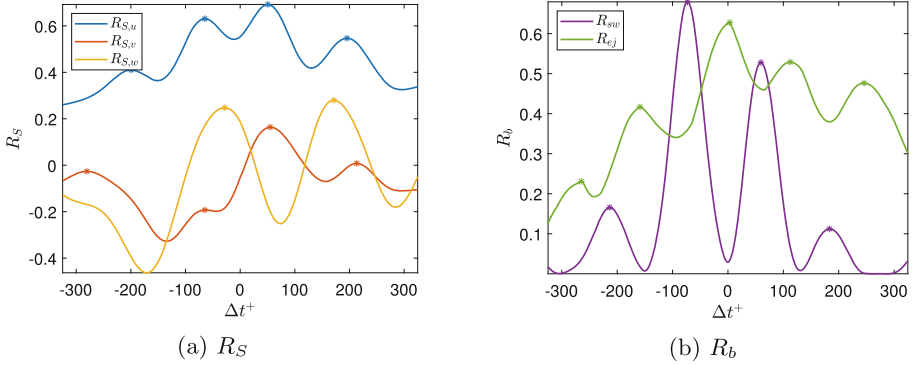
(a) R_S (b) R_b

Fig. 2. Correlation coefficients of large-scale features shown in Fig. 1.

Table 1. Correlation coefficients and inclination angles of all phenomena.

	$R_{S,max}$	Θ_S	$R_{sw,max}$	Θ_{sw}	$R_{ej,max}$	Θ_{ej}	$R_{AM,max}$	Θ_{AM}
u'	0.69	8.08°	0.68	−5.62°	0.63	65.71°	0.96	16.25°
v'	0.16	7.47°					0.86	90°
w'	0.28	2.40°	-	-	-	-	0.87	10.55°

shown in Fig. 3. A very high coherence between inner and outer distributions is observed, which is also reflected in the correlation coefficients pictured in Fig. 3d. With a maximum value of $R_{AM,u,max} = 0.96$, the streamwise amplitudes possess the highest correlation. Wall-normal and spanwise amplitudes behave very similar with $R_{AM,max} \approx 0.87$. However, the spanwise correlation function shows two distinct peaks as it was also observed with respect to the superposition. The periodicity of alternating near-wall streaks might cause this effect. Using the peak closer to a zero shift, its inclination angle is in a similar range as for the streamwise amplitudes with $\Theta_{AM,u} = 16.25°$. The near-wall wall-normal amplitudes are not shifted with respect to their outer-layer counterparts.

A study of the amplitude modulation of all three velocity components has been previously performed by Talluru et al. [12]. It must be noted that the approach to investigate the amplitude modulation is the same as reported in [9] and it was already shown in [8] that the currently used, novel approach gives a much clearer picture of the phenomenon for the streamwise components. Thus, it is not surprising that the detected degree of modulation is also higher for the two remaining velocity components. However, the study of [12] did not use near-wall components as close to the wall as in the present analysis due to experimental restrictions, which additionally hampers a precise comparison. Therefore, we applied their method to the DNS data used in the present study. The results reveal maximum correlation coefficients close to zero or even negative values. Hence, it is fair to state that the novel approach for the amplitude modulation analysis is superior in revealing this phenomenon for all three velocity components.
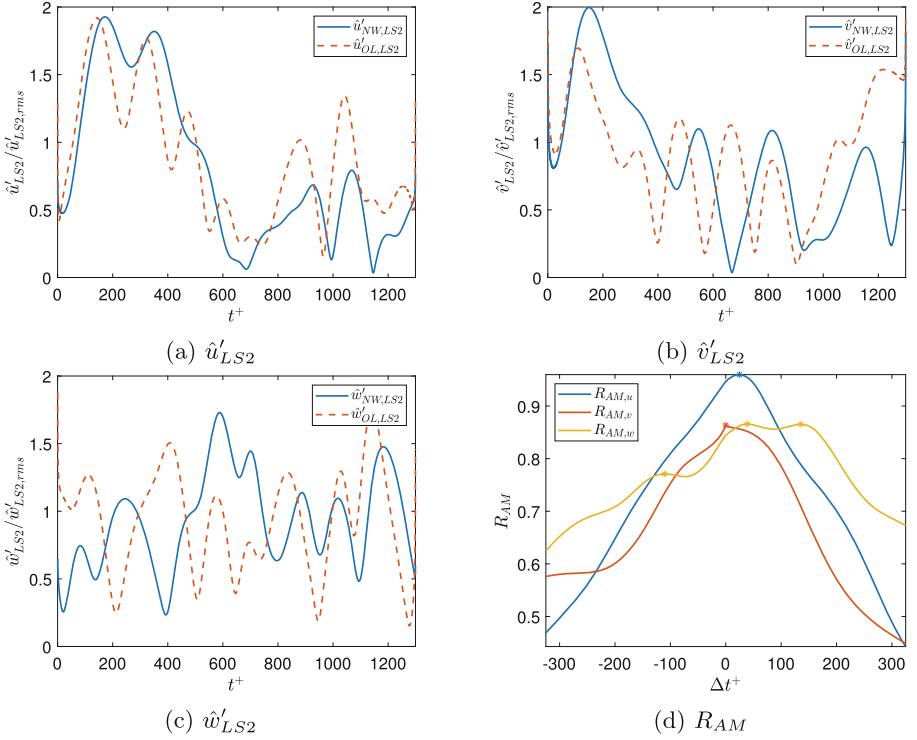
Fig. 3. Near-wall $\{\hat{u}, \hat{v}, \hat{w}\}'_{NW,LS2}$ and outer-layer large-scale amplitudes $\{\hat{u}, \hat{v}, \hat{w}\}'_{OL,LS2}$ and their correlation R_{AM}.

5 Conclusions

The inner-outer interaction is studied for a turbulent channel flow at $Re_\tau \approx 1000$. All three velocity components at the near-wall location $y^+_{NW} = 1$ and at the outer-layer location $y^+_{OL} = 123$ are considered in time-dependent, one-dimensional form. To obtain the large-scale components, the velocity fluctuations are simultaneously decomposed by a multivariate empirical mode decomposition, which ensures the alignment of scales in the individual modes. The subsequent analysis of superposition and bursting activity based on standard cross-correlation reveals a high inner-outer correlation between the large-scale streamwise components, the sweeps, and the ejections. The wall-normal and the spanwise large scales also possess a coherence between both locations but this is mathematically lost to a great extent in the applied cross-correlation due to opposite signs of the components. Hence, alternative methods are to be investigated to quantify the degree of inner-outer coherence.

Removing the influences of the superposition and bursting activity from the near-wall signals enables the analysis of the amplitude modulation. With $R_{AM} \geq 0.86$, the correlation is very high in all three directions but the stream-

wise amplitudes correlate the most. While the inclination angles of streamwise and spanwise amplitude modulation are similar and comparable to the effects of superposition, the spanwise modulation indicates a zero shift between inner and outer amplitudes. The high degree of amplitude modulation across all velocity components deviates from the findings in other studies and reveals the superior performance of the methodical approach introduced by Mäteling et al. [8].

References

1. Altıntaş, A., Davidson, L., Peng, S.: A new approximation to modulation-effect analysis based on empirical mode decomposition. Phys. Fluids **31**(2), 025117 (2019)
2. Graham, J., Kanov, K., Yang, X., Lee, M., Malaya, N., Lalescu, C., Burns, R., Eyink, G., Szalay, A., Moser, R., et al.: A web services accessible database of turbulent channel flow and its use for testing a new integral wall model for LES. J. Turbul. **17**(2), 181–215 (2016)
3. Huang, N.E., Shen, Z., Long, S.R., Wu, M.C., Shih, H.H., Zheng, Q., Yen, N.C., Tung, C.C., Liu, H.H.: The empirical mode decomposition and the Hilbert spectrum for nonlinear and non-stationary time series analysis. Proc. R. Soc. London Ser. A Math. Phys. Eng. Sci. **454**(1971), 903–995 (1998)
4. Jiménez, J.: Cascades in wall-bounded turbulence. Ann. Rev. Fluid Mech. **44**, 27–45 (2012)
5. Liu, H.Y., Bo, T.L., Liang, Y.R.: The variation of large-scale structure inclination angles in high Reynolds number atmospheric surface layers. Phys. Fluids **29**(3), 035104 (2017)
6. Marusic, I., Mathis, R., Hutchins, N.: High Reynolds number effects in wall turbulence. Int. J. Heat Fluid Flow **31**, 418–428 (2010)
7. Marusic, I., Baars, W.J., Hutchins, N.: Scaling of the streamwise turbulence intensity in the context of inner-outer interactions in wall turbulence. Phys. Rev. Fluids **2**(10), 100502 (2017)
8. Mäteling, E., Klaas, M., Schröder, W.: Detection of small-scale/large-scale interactions in turbulent wall-bounded flows. Phys. Rev. Fluids **5**(11), 114610 (2020)
9. Mathis, R., Hutchins, N., Marusic, I.: Large-scale amplitude modulation of the small-scale structures in turbulent boundary layers. J. Fluid Mech. **628**, 311–337 (2009)
10. Mathis, R., Hutchins, N., Marusic, I.: A predictive inner-outer model for streamwise turbulence statistics in wall-bounded flows. J. Fluid Mech. **681**, 537–566 (2011)
11. Rehman, N., Mandic, D.P.: Multivariate empirical mode decomposition. Proc. R. Soc. A Math. Phys. Eng. Sci. **466**(2117), 1291–1302 (2010)
12. Talluru, K., Baidya, R., Hutchins, N., Marusic, I.: Amplitude modulation of all three velocity components in turbulent boundary layers. J. Fluid Mech. **746**, 1–11 (2014)